Sensors and Materials, Vol. 38, No. 10 (2026) 6253–6274
MYU Tokyo

S & M 4679

Modal Verification and Structural Strength Analysis of an Autonomous Bus Chassis

Chang-Sheng Lin,[1*] Wen-Chen Yang,[2] and Kuan-Chi Lin[3]

[1]Department of Mechanical Engineering, National Kaohsiung University of Science and Technology, Kaohsiung, Taiwan
[2]Wistron Corporation, New Taipei City, Taiwan
[3]United Microelectronics Corporation, Hsinchu, Taiwan

(Received July 21, 2026; accepted September 29, 2026)

Keywords: experimental modal analysis (EMA), finite element analysis (FEA), modal verification, bending stiffness, torsional stiffness

In this paper, experimental modal analysis (EMA) is carried out using the actual structure of an autonomous bus chassis, and the corresponding finite element model (FEM) is verified by comparing the modal parameters obtained from EMA and finite element analysis (FEA). In EMA, impulse force is applied to the structure through an impact hammer, which has the characteristics of broadband containing frequency content around the excited structure modes of interest. We use the contact condition to replace the bolts and rivets of the chassis structure through FEA, and then to reduce the number of finite elements and improve the computational efficiency. The reliability of FEM is judged by comparing modal-estimation results obtained from EMA and FEA. The error of natural frequencies and the modal assurance criterion between modal shapes through EMA and FEA are used to verify the consistency of modal parameters. On the basis of comparison results to determine the reliability of FEM, the bending stiffness, torsional stiffness, and strength of the chassis structure are evaluated by applying corresponding boundary and loading conditions, and these values are served as safety indicators for the chassis structure.

1. Introduction

With the advancement of modern transportation technologies, increasing attention has been devoted to the safety and reliability of vehicle structures. To ensure structural integrity and occupant safety, engineers routinely perform numerical analyses and evaluations during the design stage. However, the accuracy of computer-aided engineering simulations largely depends on the fidelity of numerical models. Therefore, experimental validation procedures are often conducted to verify and update finite element (FE) models. Zaman *et al.*[1] performed FE model updating for an off-road vehicle and validated the numerical model through experimental modal

*Corresponding author: e-mail: changsheng@nkust.edu.tw
https://doi.org/10.18494/SAM6538

ISSN 0914-4935 © MYU K.K.

analysis (EMA). By refining the FE model, the discrepancies between the natural frequencies obtained from EMA and finite element analysis (FEA) were reduced, whereas the modal assurance criterion (MAC) was employed to confirm the consistency between the numerical and experimental mode shapes. Schedlinski *et al.*[2] conducted modal testing on a body-in-white structure, where air springs were installed beneath the vehicle body to simulate free-free boundary conditions. EMA was carried out using a roving hammer and fixed accelerometer configuration, and the correlation between the measured and predicted frequencies and mode shapes was subsequently evaluated using the MAC.

In practical FE modeling, the boundary conditions and constraints adopted in simulations often differ from those of actual structures, which may compromise the reliability of numerical results. Consequently, modal testing involving impulse excitation, structural response measurement, and frequency response function (FRF) calculation can be utilized to validate material properties, boundary conditions, and contact definitions within FE models. Orlowitz and Brandt[3] performed both EMA and operational modal analysis on a suspended plexiglas plate. Correlation functions were employed to verify the effectiveness of the external excitation, and the modal parameters obtained from the two approaches were compared. The results demonstrated a high degree of agreement, indicating the reliability of the material properties used in the numerical model. Sani *et al.*[4] investigated a vehicle chassis using impact hammer excitation and tri-axial accelerometers, with the structure suspended by elastic ropes on a test rig to approximate free-free conditions. Two dominant modal characteristics corresponding to different planar directions were identified, and the discrepancies in natural frequencies were found to be within 5%. Chen *et al.*[5] carried out the modal identification of a large-scale bridge using excitation sources in different directions combined with tri-axial accelerometers. Various excitation configurations successfully excited longitudinal, transverse, and torsional modes, and the identified natural frequencies exhibited discrepancies of less than 2%, with good agreement in mode shapes.

Following model validation, appropriate boundary and loading conditions can be applied to evaluate the structural performance of a chassis through stiffness and strength analyses. Li and Feng[6] investigated the stiffness characteristics of a vehicle structure by constraining the degrees of freedom at the suspension mounting locations and applying the corresponding loads. The torsional deformation behavior of the structure was subsequently characterized through torsional angle curves, thereby providing insight into the structural rigidity and overall mechanical performance.

The main contributions of this study are summarized as follows. First, an EMA procedure is established for a large-scale autonomous bus chassis under suspended free-free-like conditions. Second, the FE model is correlated with experimental modal parameters using natural-frequency errors and the MAC. Third, the correlated FE model is employed to quantitatively evaluate the bending stiffness, front and rear torsional stiffness, and structural strength of the chassis. Finally, the proposed numerical–experimental framework provides a practical approach for identifying discrepancies between numerical predictions and the actual structure before subsequent structural performance evaluations.

2. Research Method

In this study, FEA and EMA were employed to validate the geometric model of the autonomous bus chassis structure. The modal characteristics were computed using the commercial software ANSYS Workbench. In addition, harmonic response analysis was performed to determine the displacement responses under harmonic excitation over a range of frequencies, thereby obtaining the frequency response functions (FRFs) of the structure. The mode shapes predicted by the FE model were further utilized as a reference for the planning of EMA.

After determining the measurement locations, dynamic response measurements were conducted on the physical structure. The coherence function was employed to evaluate the correlation between the excitation and response signals. Subsequently, FRFs were calculated from the measured excitation and response data, and experimental modal parameters were identified. The modal parameters obtained from FEA and EMA were then compared to assess the consistency between the numerical model and the actual structure. Specifically, natural frequencies and mode shapes were used as primary validation criteria, while the MAC was adopted as a quantitative index for evaluating the similarity between the numerical and experimental mode shapes. Upon completing the modal validation, the equivalence between the FE model and the physical structure was confirmed.

In this study, a combined numerical and experimental approach is adopted to validate the FE model of an autonomous bus chassis through EMA. After establishing the equivalence between the numerical model and the physical structure, static analyses are performed to evaluate the bending stiffness, torsional stiffness, and structural strength under full-load conditions. The obtained results provide quantitative indicators for assessing the structural integrity and safety of the chassis. The overall workflow of modal validation and structural strength assessment is illustrated in Fig. 1.

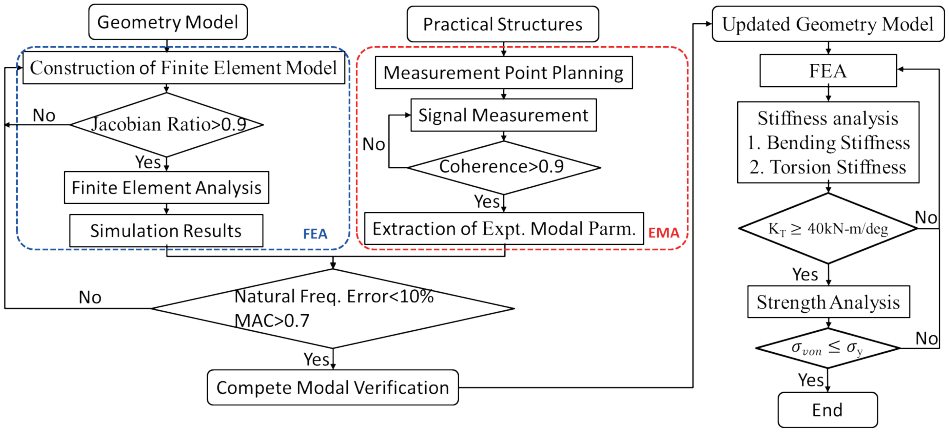


Fig. 1. (Color online) Flowchart of modal testing and validation procedure.

2.1 FEA

In this study, the commercial FE software ANSYS Workbench was employed to perform structural modal analysis. The natural frequencies and mode shapes of the structure under free-free boundary conditions were computed. The obtained modal parameters were further used as a reference for experimental design. In addition, harmonic response analysis was conducted to determine the FRFs between different excitation and response locations.

The target structure investigated in this study is the chassis of an autonomous bus, as shown in Fig. 2. The main materials of the lower beams are AL-6082 and SS400, whereas the suspension brackets and suspension tower mounts are made of SS400 and 206.0-T7, respectively. The corresponding material properties are listed in Table 1. The FE geometric model of the chassis structure is illustrated in Fig. 3.



Fig. 2. (Color online) Actual chassis structure of autonomous bus.

Table 1
Mechanical properties of materials used in chassis components.

		Properties		
		Density (kg/m^3)	Young's modulus (GPa)	Poisson's ratio (-)
Material	AL-6082	2710	70	0.3
	SS400	7850	210	0.3
	206.0-T7	2890	70	0.3

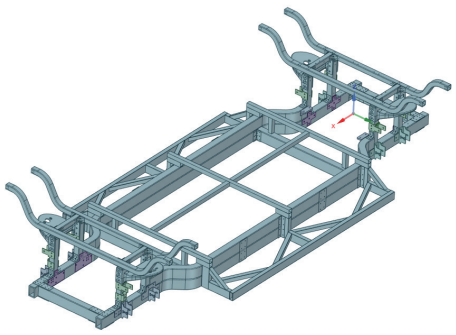


Fig. 3. (Color online) FE geometric model of chassis structure.

In this study, a FE model was developed to discretize the complex and continuous structural system into a finite number of elements. Since the inclusion of fasteners such as bolts and rivets will require a significantly higher number of elements and consequently increase computational cost, all fasteners in the vehicle assembly were removed and their effects were represented using appropriate contact conditions to reduce computational time.

For fasteners and welded interfaces, fully constrained boundary conditions were applied to better represent the actual structural behavior and to prevent any relative displacement. The mesh quality was evaluated on the basis of the Jacobian ratio, and the overall mesh quality was maintained at approximately 0.95. This value is higher than the criterion of 0.9 defined in this study, indicating that the FE model exhibits acceptable mesh quality and reliability. The FE geometric model is shown in Fig. 4, and the corresponding model information is summarized in Table 2.

Note that, to reduce the computational cost, individual bolts and rivets were not explicitly modeled. The corresponding interfaces were represented using constrained no-slip contact conditions. Although this approach efficiently reproduces the overall connectivity of the chassis, it may overestimate the local stiffness of actual bolted and riveted joints because joint compliance is not explicitly modeled. This simplification is therefore considered a possible contributor to the discrepancies between the experimentally measured and numerically predicted modal frequencies, particularly for global bending and torsional modes.

2.2 EMA

EMA is employed to identify the modal parameters of a real structure. In this approach, a broadband impulse excitation is applied to the structure, and the corresponding response signals are measured. Both excitation and response signals are processed using spectral analysis



Fig. 4. (Color online) FE geometric model of chassis structure.

Table 2
FE modeling parameters.

Element information	
Element type	2nd oder tetrahedron
	2nd oder hexahedron
Element quantity (−)	401390
Node number (−)	837330

software, where fast Fourier transform (FFT) is applied independently to compute the FRF. The modal parameters of the actual chassis structure are then estimated through the curve fitting of FRFs using modal analysis software.

During the experimental design stage, the mode shapes obtained from FEA are used as a reference to determine an adequate number of measurement points, ensuring that the targeted mode shapes can be effectively captured. This also allows the required measurement bandwidth to be appropriately defined.

In practical measurements of structural dynamic responses, external environmental vibrations and other sources of interference may introduce noise, thereby affecting the reliability of the measured signals. To evaluate whether the response signals are truly induced by the excitation input, the coherence function, denoted as γ^2, is used to quantify the degree of correlation between the excitation and response signals, as expressed in Eq. (1).

$$\gamma^2(f) = \frac{\left|G_{xf}(f)\right|^2}{G_{ff}(f)G_{xx}(f)} \tag{1}$$

Here, $G_{ff}(f)$, $G_{xx}(f)$, and $G_{xf}(f)$ denote the auto power spectral density (PSD) function of the response, the auto PSD function of the excitation, and the cross PSD function between the response and the excitation, respectively. When the correlation between the excitation and response signals is high, the coherence function approaches unity; conversely, when the correlation between the input and output signals is low, the coherence function tends toward zero.

After evaluating the coherence function to verify the correlation between the measured response and excitation signals, the FRF of the system is subsequently computed using $G_{af}(f)$ and $G_{ff}(f)$. The formulation of the FRF is given in Eq. (2).

$$H_{af}(f) = \frac{G_{af}(f)}{G_{ff}(f)} \tag{2}$$

The system responses corresponding to different excitation degrees of freedom were obtained using Eq. (2). Subsequently, the modal parameters of the frequency response functions were identified using ME'scope software.

2.2.1 Experimental setup for modal testing

The experimental setup employed a PCB 086D20 impact hammer equipped with a rubber tip to excite the chassis structure. To ensure that the modal responses within the target frequency bandwidth can be effectively captured, the effective frequency range of different hammer tips provided by PCB was referenced, as shown in Fig. 5. It can be observed that, at the 20 dB energy decay level (intersection of the dashed and red lines), the rubber tip provides a sufficient effective bandwidth to satisfy the measurement requirements of this study.

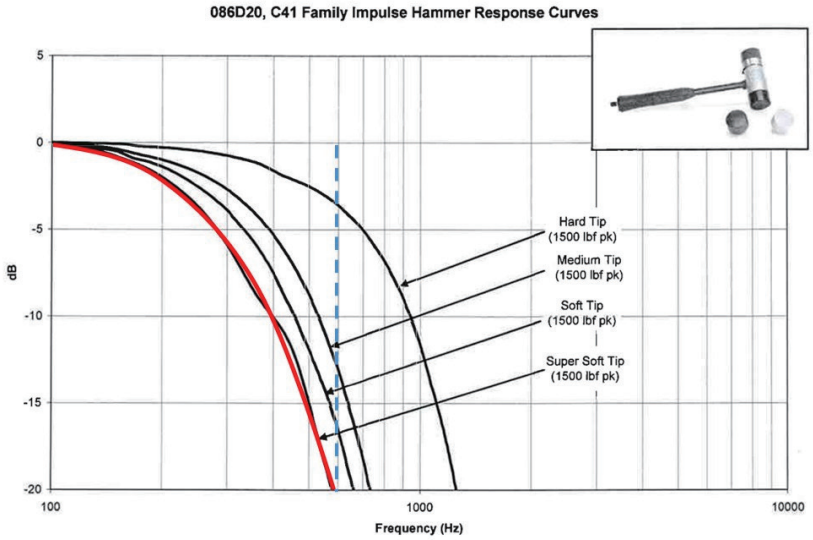


Fig. 5. (Color online) Auto PSD of impact hammer excitation signal.

A tri-axial accelerometer was used to measure the structural responses, enabling three-dimensional degrees of freedom to be captured and allowing the spatial modal characteristics of the chassis in different planes to be identified. The data acquisition system consisted of an NI 9234 module combined with m+p spectral analysis software for signal acquisition and processing. The relevant experimental equipment, models, and specifications are summarized in Table 3.

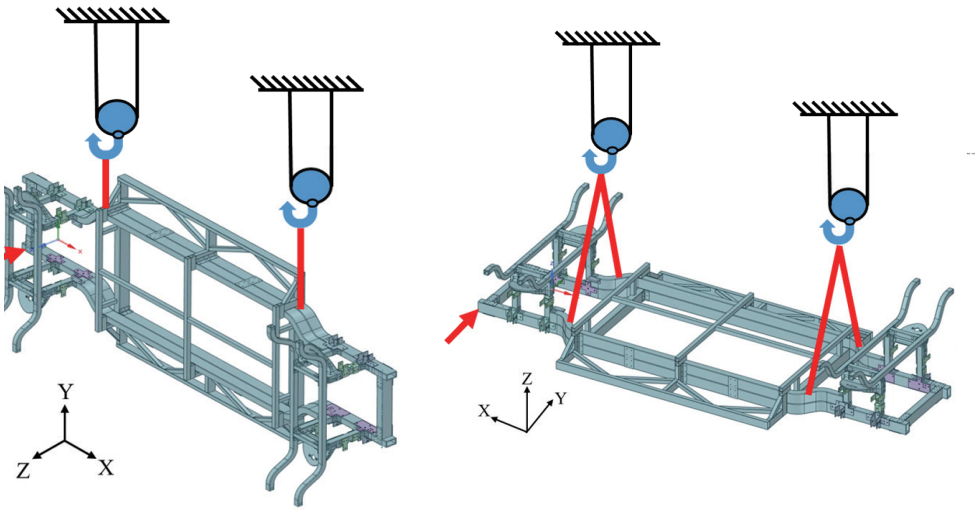
To effectively capture vibration modes in different planes, excitation in multiple directions was planned to obtain the corresponding structural responses. In this experiment, two test configurations were designed to excite vibration modes in the *Y*- and *Z*-directions. The schematic setups are illustrated in Fig. 6. In this configuration, the suspension direction was arranged to be orthogonal to the excitation direction to approximate free-free boundary conditions for modal analysis. During the actual measurements, the chassis structure was suspended using an overhead crane, as shown in Fig. 7.

2.2.2 Layout of measurement points for EMA

The modes of interest in this study are primarily global vibration modes. The measurement point layout was designed with reference to the mode shapes obtained from FEA. A total of 49 measurement points were selected, corresponding to 147 measurement degrees of freedom by acquiring dynamic responses in three orthogonal directions. These measurements enable the characterization of the spatial modal behavior of the structure, as shown in Fig. 8. The measurement locations were selected on the basis of preliminary FEA mode shapes, with

Table 3
(Color online) Experimental equipment, models, and specifications.

Equipment and Model	Specifications
 Instrumented impact hammer (PCB 086D20)	Sensitivity: 0.23 mV/N Tip: super soft tip Frequency range: 500 Hz
 Tri-axial accelerometer (DJB AT/18)	Sensitivity: 10 mV/g Frequency range: 1–12 kHz Weight: 1.2 g
 Data acquisition system (DAQ) (NI 9234)	Channels: 4 Max. Sampling rate: 51.2 kHz



(a) (b)

Fig. 6. (Color online) Schematic of chassis suspension setup in (a) *Y*- and (b) *Z*-directions.



(a) (b)

Fig. 7. (Color online) Experimental setup of chassis suspension in (a) *Y*- and (b) *Z*-directions.

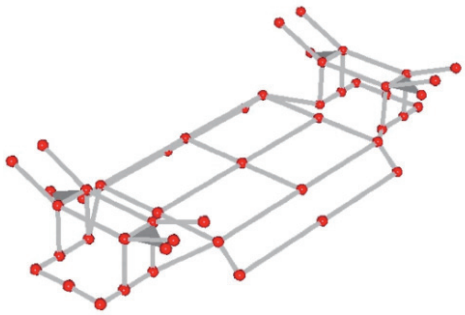


Fig. 8. (Color online) Measurement point distribution of experimental model.

emphasis on regions exhibiting representative global modal deformation. A total of 49 locations and 147 measurement degrees of freedom were employed. No formal sensor-placement optimization algorithm was applied. Instead, the adequacy of the measurement layout was assessed through the quality of the measured FRFs, coherence functions, complex mode indicator function (CMIF) results, and subsequent MAC comparison with the FE mode shapes. Formal sensor-placement optimization may further improve the experimental modal identification and is therefore considered a potential direction for future work.

2.3 Modal verification

In the modal parameter comparison, natural frequencies can be directly evaluated on the basis of percentage errors. However, for mode shapes, a visual comparison between EMA and FEA results is insufficient, particularly for chassis structures exhibiting spatial vibration modes.

To more accurately assess the validity of modal identification between EMA and FEA, in addition to the natural frequency error, the MAC[7] is employed to quantify the correlation between the FE model and the actual chassis structure. The definition of the MAC is given in Eq. (3).

$$MAC(A,X)=\frac{\left|(\phi_{iA})^{T}(\phi_{jX})^{*}\right|^{2}}{(\phi_{iA})^{T}(\phi_{iA})^{*}(\phi_{jX})^{T}(\phi_{jX})^{*}} \tag{3}$$

Here, the superscript T denotes the transpose operator and the superscript $*$ represents the complex conjugate operator. ϕ_{iA} and ϕ_{jX} are the mode shapes obtained from an analytical procedure (harmonic/FEA) and EMA, respectively. When the correlation between two mode shapes is high, the MAC value approaches unity; conversely, when the correlation is low, the MAC value approaches zero.

Note that conventional criteria for modal validation typically adopt thresholds of a natural frequency error within 5% and a MAC value greater than 0.9. However, in this study, the validation target is an autonomous bus chassis, which is a large-scale structure assembled from numerous bolted and riveted components. As a result, the modal identification process is more complex and less idealized than single-component structures. Therefore, relaxed acceptance criteria of a natural frequency error within 10% and a MAC value greater than 0.7 are adopted as validation thresholds to assess the reliability of the FE model.

2.4 Strength analysis

Stiffness refers to the resistance of a structure to deformation under applied external loads, i.e., the difficulty with which a structure undergoes deformation. Stiffness can generally be categorized into bending and torsional modes. Under loading conditions, a structure primarily experiences bending deformation, whereas during vehicle operation over road irregularities or during cornering, the structure is subjected to roll deformation. Therefore, bending stiffness and torsional stiffness are commonly adopted as key indicators for evaluating the structural safety of vehicle designs.

Strength is defined as the ability of a metallic material to resist permanent deformation and fracture under external loading. Through structural analysis under prescribed loading conditions, the stress and deformation responses can be predicted in advance, allowing the evaluation of whether the structure can safely withstand the applied loads.

2.4.1 Boundary conditions for bending stiffness analysis

In the bending load analysis, a static loading condition of the vehicle was simulated. At the four suspension tower mount locations where shock absorbers are connected, the shock absorbers were assumed to be non-functional. Therefore, no displacement was allowed at the suspension tower mounts in any direction. The translational degrees of freedom (UX, UY, and

UZ) at the center surfaces of the suspension tower mounts were fully constrained. A vertical concentrated load of 1000 N in the negative *Z*-direction was applied at the midpoint of the two main beams.

2.4.2 Bending stiffness calculation

Bending stiffness is one of the key performance indicators used to evaluate the resistance of a chassis structure against bending deformation. When a beam is subjected to a vertical load, the resulting deformation is linearly proportional to the applied load, in accordance with Hooke's law. Bending stiffness is determined on the basis of the deformation at the loading location. As shown in Fig. 9, the bending stiffness K_B of the chassis structure is calculated from the applied load F and the corresponding deformation δ, as expressed in Eq. (4).

$$K_B = \frac{F}{\delta} \tag{4}$$

Here, F denotes the total applied load on the structure and δ represents the deformation of the chassis structure under loading conditions.

For a chassis structure consisting of two main beams, the overall bending stiffness K_B of the vehicle can be calculated as

$$K_B = \frac{F_1 + F_2}{\left(\frac{\delta_1 + \delta_2}{2}\right)}. \tag{5}$$

Here, F denotes the total applied load and δ represents the displacement of the two beams.

2.4.3 Boundary conditions for torsional stiffness analysis

In the front torsional analysis, equal and opposite vertical loads of 1000 N in the negative *Z*-direction, acting along the same line, were applied at the center surfaces of the two front suspension tower mounts. The center surfaces of the two rear suspension tower mounts were fully constrained in all translational degrees of freedom (UX, UY, and UZ).

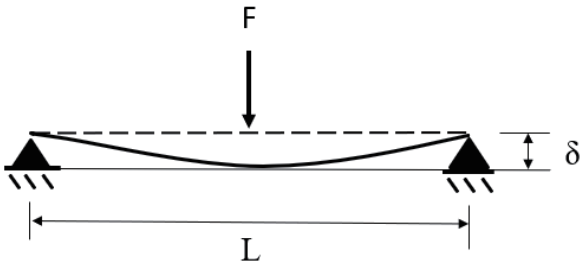


Fig. 9. Schematic of bending stiffness evaluation.

In the rear torsional analysis, the boundary conditions were reversed. The center surfaces of the two front suspension tower mounts were fully constrained in all translational degrees of freedom (UX, UY, and UZ), whereas equal and opposite vertical loads of 1000 N in the negative Z-direction, acting along the same line, were applied at the center surfaces of the two rear suspension tower mounts.

2.4.4 Torsional stiffness calculation

Torsional stiffness is one of the key performance indicators used to evaluate the resistance of a vehicle structure to torsional deformation. As illustrated in Fig. 10, the structure undergoes twisting when subjected to torsional loading, resulting in the torsional angle θ determined as

$$\theta = \tan^{-1}\left(\frac{d}{L}\right). \tag{6}$$

Here, d denotes the relative deformation between the two suspension tower mounts and L is the distance between the centers of the suspension tower mounts. The torsional stiffness K_T is defined as the ratio of the applied torque T to the resulting torsional angle θ. Accordingly, the torsional stiffness can be calculated as

$$K_T = \frac{T}{\theta} = \left(\frac{F \times L}{\theta}\right). \tag{7}$$

2.4.5 Boundary conditions for structural strength analysis

In the structural strength analysis, the center surfaces of the four suspension tower mounts were fully constrained in all translational degrees of freedom (UX, UY, and UZ). The loading conditions considered in this study include the maximum acceleration and deceleration of approximately 1 g during vehicle driving and braking, the self-weight of the vehicle body (W), and the total vehicle payload ranging from 10000 to 50000 N (corresponding to the maximum allowable payload of 4500 kg, denoted as F). An acceleration load of approximately 9.81 m/s² (1

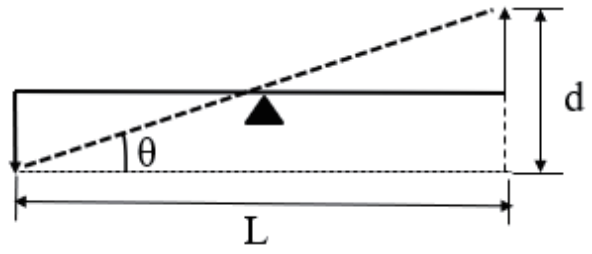


Fig. 10. Schematic of torsional stiffness evaluation.

g) was applied in the vehicle longitudinal direction to represent the inertial effect associated with the prescribed driving/braking condition. The acceleration was treated as a body inertial load in the FE model rather than as an additional concentrated external force. The self-weight and payload were included simultaneously in the corresponding load case.

2.4.6 Structural strength verification

Structural strength analysis is a key indicator used to evaluate the ability of a vehicle structure to resist material failure. When the chassis is subjected to 1 g acceleration/deceleration induced by driving and braking, the self-weight of the vehicle body, and the full vehicle payload, the resulting stresses should not exceed the yield strength of any constituent material. This ensures that the structural integrity is maintained and that no permanent deformation occurs under the specified loading conditions. The yield strengths of the corresponding materials are listed in Table 4.

3. Results and Discussion

3.1 Modal verification

After acquiring the response signals of the chassis structure, the coherence function between the response and excitation signals was calculated to evaluate whether the observed response peaks in the FRFs were truly induced by external excitation or were numerical artifacts generated during the curve fitting of higher-order components. In addition, the phase characteristics of the structural modes, particularly the 180° phase transition behavior, were utilized to effectively extract the modal parameters.

The magnitude–phase relationships, coherence functions, and curve-fitted FRFs for the *Y*- and *Z*-direction suspension configurations of the chassis are shown in Figs. 11 and 12, respectively. As shown in the coherence and phase plots, the coherence values remained below 0.9 in the low-frequency range of approximately 0–10 Hz, while the corresponding phase transitions did not reach 180°. Therefore, this frequency range may be described as a low-frequency suspension/rigid-body disturbance region, rather than definitively attributing it exclusively to rigid-body modes, and was excluded during the curve-fitting process for modal parameter identification.

For the experimental results of the *Y*- and *Z*-direction suspension configurations [Figs. 11(a), 11(b), 12(a), and 12 (b)], it can be observed that each identified mode in the FRFs corresponds to regions where the coherence function exceeds 0.9 and where a 180° phase transition occurs.

Table 4
Yield strengths of materials.

Material type	Yielding stress (MPa)
6082	110
SS400	245
206.0-T7	345

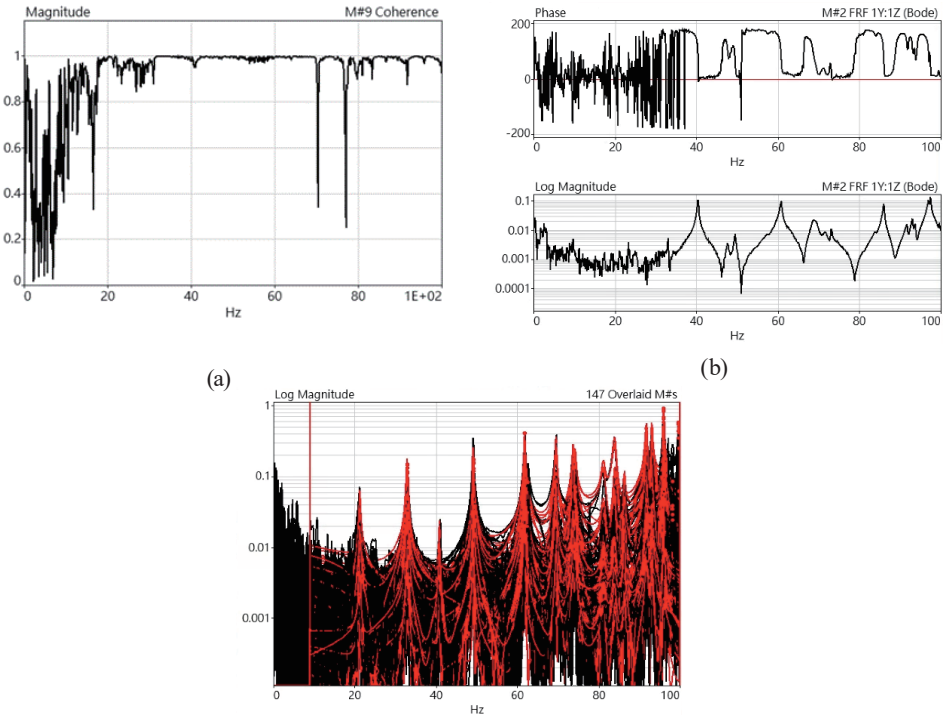


Fig. 11. (Color online) (a) Coherence function, (b) magnitude–phase diagram, and (c) curve-fitted frequency response functions within measured bandwidth obtained from *Y*-direction suspension test of chassis.

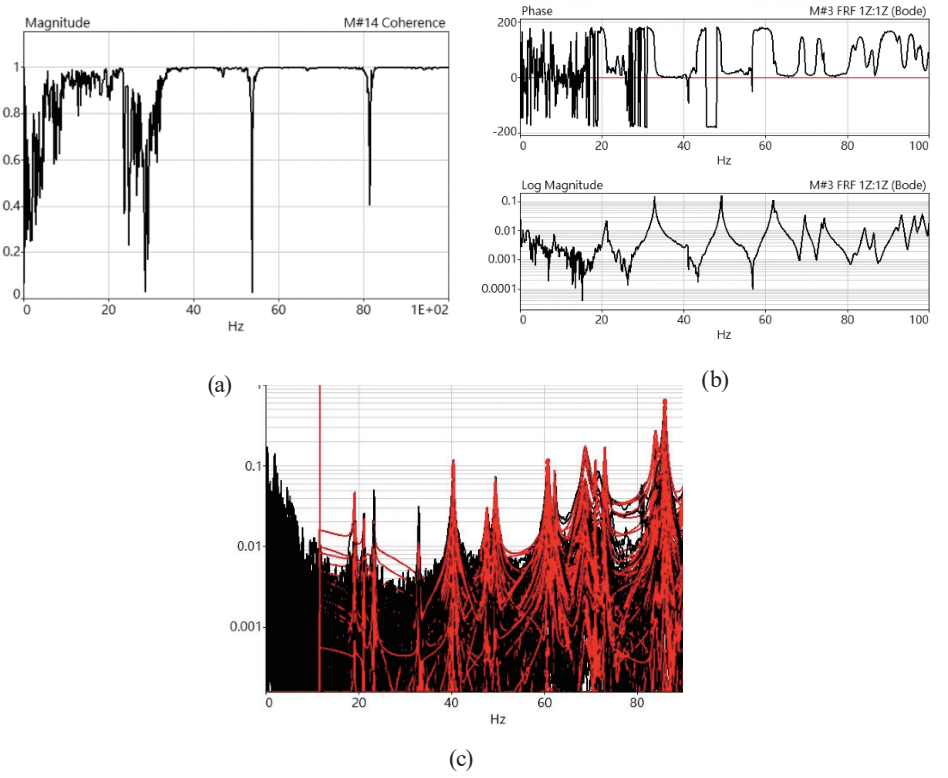


Fig. 12. (Color online) (a) Coherence function, (b) magnitude–phase diagram, and (c) curve-fitted frequency response functions within measured bandwidth obtained from *Z*-direction suspension test of chassis.

Figures 11(c) and 12(c) present the overlaid FRFs of 147 measurement degrees of freedom. The CMIF was also employed to identify the dominant modes excited in the experiment.

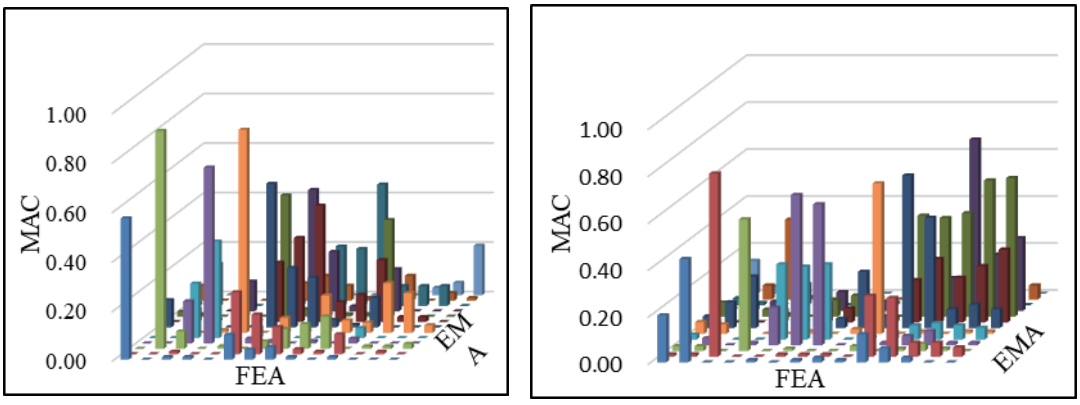
The modal parameters were extracted by curve-fitting the FRFs calculated using spectral analysis software. A comparison between the modal parameters obtained from EMA and FEA was then conducted. The MAC values corresponding to different excitation directions are shown in Fig. 13.

The natural frequency errors and MAC values obtained from different excitation configurations were summarized, and the corresponding modes were selected and are listed in Table 5. In terms of natural frequency, the errors of the first, second, and fifth modes were relatively large, whereas those of the remaining modes were all within 10%. Regarding the MAC values, only the seventh mode was lower than the acceptance threshold of 0.7.

The large frequency discrepancies observed in Modes 2 and 5 are considered primarily related to the idealization of structural joints and boundary conditions. In the FE model, the original bolts and rivets were removed and their structural effects were represented using simplified interface constraints. In contrast, the actual chassis contains numerous bolted and riveted connections, whose local compliance and contact behavior may affect the global bending and torsional characteristics.

In addition, the experimental structure was suspended from an overhead crane to approximate free-free conditions. Although this configuration reduces the effect of external constraints, the actual suspension system cannot be regarded as a mathematically perfect free-free boundary condition. Small differences in suspension flexibility, mass distribution, manufacturing tolerances, and local joint conditions may therefore affect the experimentally identified frequencies.

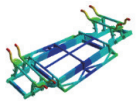
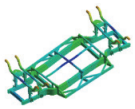
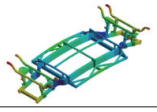
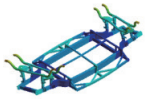
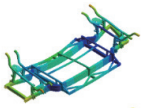
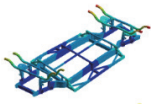
The discrepancy may be particularly pronounced for Modes 2 and 5 because these modes involve global *X*–*Z*-plane bending and twisting, respectively, which are more sensitive to the stiffness distribution of structural joints and interfaces. For Mode 7, the natural-frequency error is only 5.10%, whereas its MAC value is 0.58. This indicates that the predicted natural frequency is reasonably close to the experimental value, but the spatial distribution of the measured and



(a) (b)

Fig. 13. (Color online) MAC values obtained from (a) *Y*- and (b) *Z*-direction suspension test of chassis.

Table 5
(Color online) Comparison of modal parameters between FEA and EMA.

Mode no.	Mode shape	Modal parameters	
		EMA	FEA
1	1st *X*–*Y* Plane Twist Mode	21.14 Hz	23.72 Hz
			
		Freq. error: 12.20%	
		MAC:0.77	
2	1st *X*–*Z* Plane Bending Mode	23.23 Hz	31.61 Hz
			
		Freq. error: 36.07%	
		MAC:0.78	
3	1st *X*–*Y* Plane Bending Mode	32.81 Hz	33.50 Hz
			
		Freq. error: 2.10%	
		MAC:0.96	
4	2nd *X*–*Y* Plane Twist Mode	49.10 Hz	51.45 Hz
			
		Freq. error: 4.79%	
		MAC:0.84	
5	1st *X*–*Z* Plane Twist Mode	40.33 Hz	56.63 Hz
			
		Freq. error: 40.42 %	
		MAC: 0.75	
6	2nd *X*–*Y* Plane Bending Mode	61.74 Hz	61.92 Hz
			
		Freq. error: 0.29%	
		MAC: 0.83	
7	2nd *X*–*Z* Plane Twist Mode	69.43 Hz	72.97 Hz
			
		Freq. error: 5.10%	
		MAC: 0.58	

predicted modal deformations is less consistent. This behavior may result from differences in local deformation, joint flexibility, measurement-point discretization, and the sensitivity of higher-order modes to small structural or boundary-condition variations.

Note that the super-soft rubber tip was selected because the primary objective of EMA was to identify the global structural modes within the investigated low-frequency range. The target modes reported in this study were located approximately between 21 and 73 Hz. Therefore, the required excitation bandwidth was substantially lower than the nominal 500 Hz effective bandwidth shown in Fig. 5. The selection was not based on the requirement to excite the structure uniformly over the entire 500 Hz range. Instead, the relevant criterion was whether sufficient excitation energy was available around the frequencies of interest. The excitation spectrum shown in Fig. 5 was therefore examined to confirm that the impact hammer provided measurable excitation energy throughout the frequency range containing the target modes. In addition, the measured FRFs, coherence functions, and CMIF results were used to verify that the corresponding modal responses were actually excited and identifiable. In particular, Modes 6 and 7 were experimentally identified at 61.74 and 69.43 Hz, respectively, demonstrating that the excitation was sufficient to obtain measurable structural responses in the 60–80 Hz range.

3.2 Bending stiffness analysis

When a vertical concentrated load of 1000 N was applied at the midpoint of the two main beams, the maximum displacement occurred at the loading location, with an absolute displacement of 0.007 mm. No displacement was observed at the four constrained suspension tower mounts. The bending stiffness analysis is illustrated in Fig. 14.

By substituting the total applied load and the corresponding displacement into Eq. (5), the bending stiffness was calculated to be 285,714 N/mm.

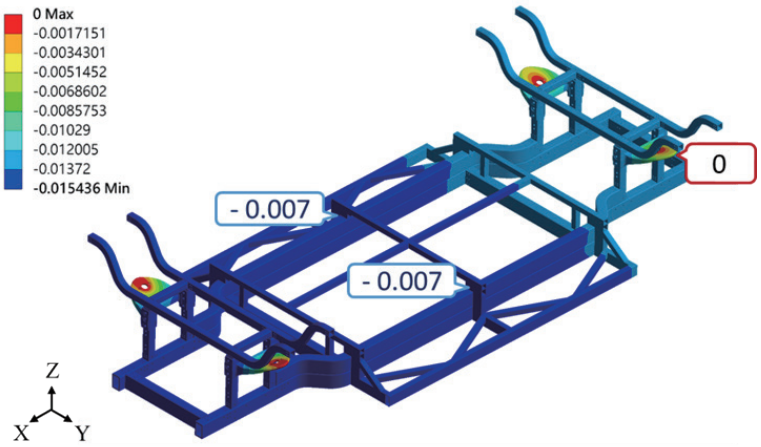


Fig. 14. (Color online) FE prediction of bending deformation of autonomous bus chassis under 1000 N vertical concentrated load applied at midpoint of two main beams, with four suspension tower mounts fully constrained.

3.3 Front torsional stiffness analysis

On the basis of the results of the front torsional stiffness analysis, equal and opposite loads were applied at the front suspension tower mounts, while the rear suspension tower mounts were fully constrained with no displacement allowed. Under this boundary condition, a clear torsional deformation behavior was observed at the front end of the structure.

The displacement of the left front suspension tower mount was −0.177 mm, whereas that of the right front suspension tower mount was 0.193 mm. The torsional stiffness analysis is illustrated in Fig. 15.

The displacements of the two front suspension tower mounts were substituted into Eq. (6) to calculate the torsional angle, which was determined to be 0.0153°. The obtained torsional angle was then substituted into Eq. (7), yielding a torsional stiffness of 90,615 N·m/deg.

In addition, 192 measurement points were selected along the vehicle body from the front to the rear to measure the displacement distribution. The measured data were used to construct a torsional angle profile along the chassis. The resulting curve illustrates the variation trend of torsional deformation along the longitudinal direction of the vehicle body, as shown in Fig. 16.

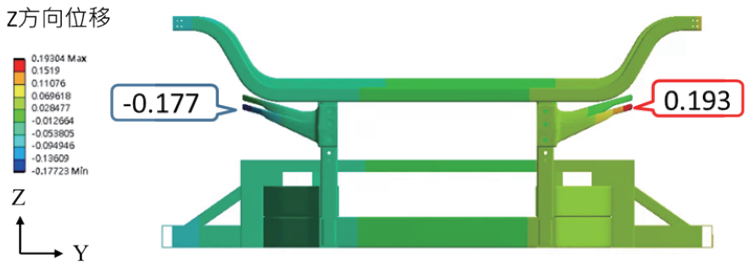


Fig. 15. (Color online) FE prediction of front torsional deformation of autonomous bus chassis under equal and opposite 1000 N vertical loads applied at front suspension tower mounts, with rear suspension tower mounts fully constrained.

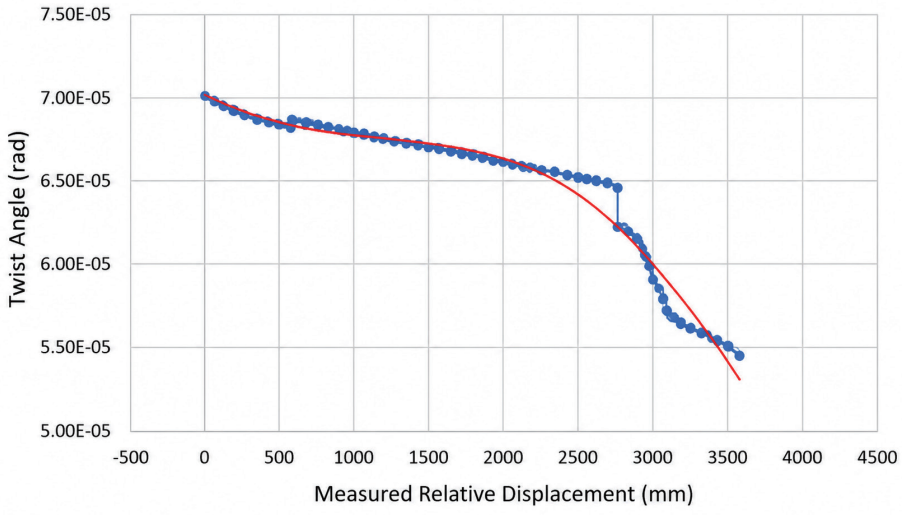


Fig. 16. (Color online) Torsional angle distribution along front section of chassis.

3.4 Rear torsional stiffness analysis

On the basis of the results of the rear torsional stiffness analysis, the front suspension tower mounts were fully constrained, whereas equal and opposite loads were applied at the rear suspension tower mounts. Under this loading condition, a clear torsional deformation tendency was observed at the rear end of the structure.

The displacement of the left rear suspension tower mount was −0.121 mm, whereas that of the right rear suspension tower mount was 0.130 mm. The torsional stiffness analysis is illustrated in Fig. 17.

The displacements of the two rear suspension tower mounts were substituted into Eq. (6) to calculate the torsional angle, which was determined to be 0.0104°. The obtained torsional angle was then substituted into Eq. (7), yielding a torsional stiffness of 133,576 N·m/deg.

In addition, 192 measurement points were selected along the vehicle body from the front to the rear to measure the displacement distribution. The measured data were used to construct a torsional angle profile along the chassis. The resulting curve illustrates the variation trend of torsional deformation along the longitudinal direction of the vehicle body, as shown in Fig. 18.

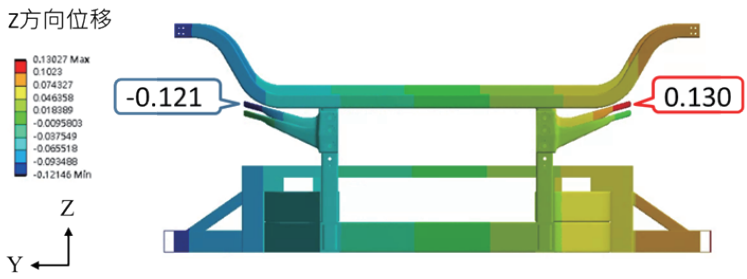


Fig. 17. (Color online) FE prediction of rear torsional deformation of autonomous bus chassis under equal and opposite 1000 N vertical loads applied at rear suspension tower mounts, with front suspension tower mounts fully constrained.

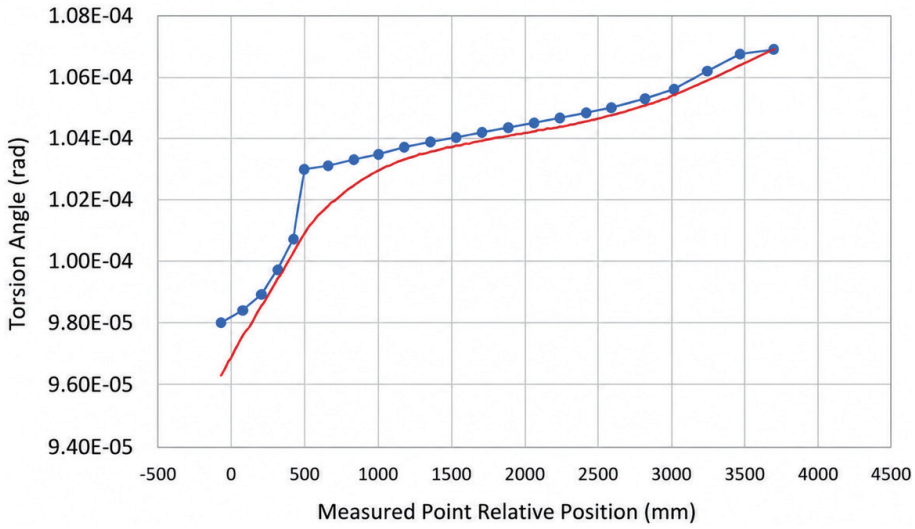


Fig. 18. (Color online) Torsional angle distribution along rear section of chassis.

3.5 Structural strength analysis

According to relevant regulations, the maximum allowable load for this type of vehicle is 4500 kg (45000 N). In this section, the applied load was increased from 10000 to 50000 N, whereas the self-weight of the vehicle body and the inertial effects corresponding to 1 g acceleration and deceleration during driving and braking were also considered as the same corresponding load case in Sect. 2.4.5.

The analysis results indicate that the maximum von Mises stress occurs at the four suspension tower mounts, with a peak stress of 69.07 MPa. The strength analysis is illustrated in Fig. 19. Further examination shows that the stress levels in all components remain below the yield strength of their respective materials. The stress variation history is presented in Fig. 20.

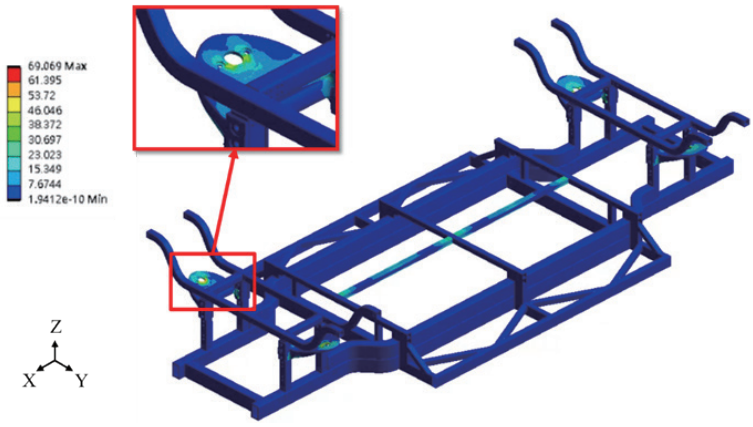


Fig. 19. (Color online) FE prediction of von Mises stress distribution in autonomous bus chassis under combined loading condition of vehicle self-weight, payload, and approximately 1 g inertial acceleration/deceleration.

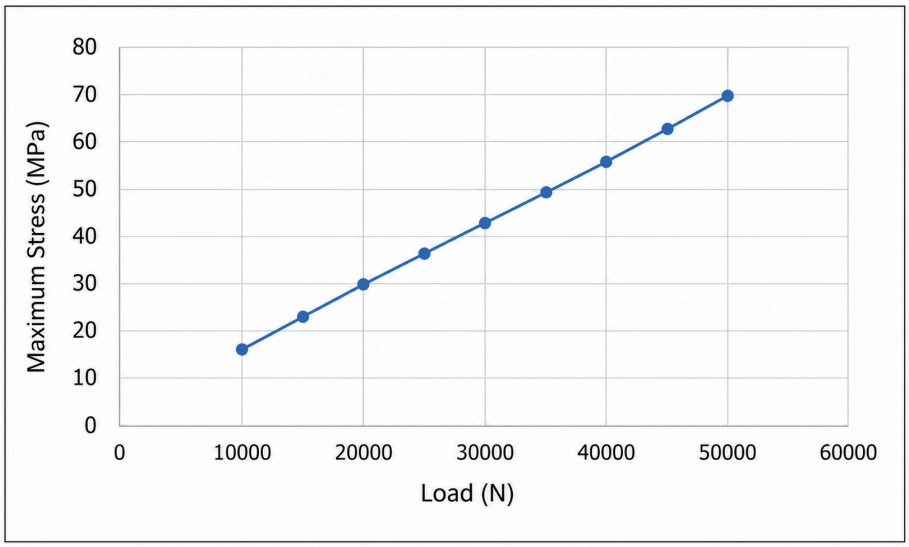


Fig. 20. (Color online) Stress variation of chassis structure.

4. Conclusions

We conducted an integrated numerical–experimental investigation on the modal characteristics and structural integrity of an autonomous bus chassis. A FE model demonstrates acceptable overall modal correlation for subsequent global structural assessment, whereas the discrepancies of Modes 2 and 5 respectively corresponding to an *X*–*Z*-plane bending mode and an *X*–*Z*-plane twisting mode are explicitly recognized as modal-verification limitations. The discrepancies in natural frequencies were generally within 10%, whereas the MAC values exceeded 0.7 for most correlated mode shapes. These results demonstrate a correlation between numerical predictions and experimental measurements, confirming the reliability and adequacy of the developed FE model. The bending and torsional stiffness characteristics of the chassis were quantitatively evaluated. The calculated front and rear torsional stiffness values were 90.6 and 133.6 kN·m/deg, respectively, indicating high global torsional rigidity under the prescribed boundary and loading conditions. The comparison with published passenger-vehicle reference values provides a qualitative indication of structural rigidity; however, because the reference vehicle category and the autonomous bus architecture are not identical, this comparison should not be interpreted as a direct regulatory compliance criterion. Further stiffness-to-weight optimization is recommended to determine whether structural mass can be reduced while maintaining the required stiffness and strength. Structural strength assessment under full-load conditions revealed that the maximum von Mises stresses in all components remained below their respective yield strengths. This indicates that no plastic deformation is expected under the considered loading scenario, confirming the adequate structural safety of the chassis design. Overall, the validated numerical model, together with stiffness and strength evaluations, provides a reliable framework for assessing the structural performance of autonomous bus chassis systems.

The engineering implication of the proposed verification procedure is that experimental modal testing can be used as an early-stage correlation procedure to identify discrepancies in the FE model before extensive static structural evaluation and design iteration. Once the numerical model has been experimentally correlated, subsequent parametric analyses can be performed numerically without requiring a physical prototype for every design modification. However, because the present study does not include a systematic comparison of development cycles with and without the proposed verification procedure, a specific percentage reduction in prototype testing or overall development time cannot be quantitatively claimed.

References

1 I. Zaman, R. A. Rahman, and H. Khalid: J. Sci. Technol. **4** (2007) 1.
2 C. Schedlinski, F. Wagner, K. Bohnert, and A. Müller: Proc. Int. Semin. Modal Analysis (KU Leuven, 2004).
3 E. Orlowitz and A. Brandt: Measurement **102** (2017) 121. https://doi.org/10.1016/j.measurement.2017.02.001
4 M. S. M. Sani, M. M. Rahman, M. M. Noor, K. Kadirgama, and M. H. N. Izham: IOP Conf. Ser.: Mater. Sci. Eng. **17** (2011) 012038. https://doi.org/10.1088/1757-899X/17/1/012038
5 G.-W. Chen, P. Omenzetter, and S. Beskhyroun: Eng. Struct. **229** (2021) 111604. https://doi.org/10.1016/j.engstruct.2020.111604
6 S. Li and X. Feng: Mech. Syst. Signal Process. **135** (2020) 106380. https://doi.org/10.1016/j.ymssp.2019.106380
7 R. J. Allemang: Sound Vib. **37** (2003) 14.

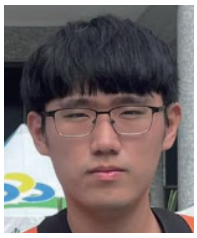
About the Authors



Chang-Sheng Lin received his Ph.D. degree from the Department of Aeronautics and Astronautics of National Cheng Kung University, Taiwan, in 2011. He joined the Faculty of National Kaohsiung University of Science and Technology, Taiwan, in 2024, where he is currently an associate professor at the Department of Mechanical Engineering. His research interests are in random vibration and modal analysis. (changsheng@nkust.edu.tw)



Wen-Chen Yang received his B.S. and M.S. degrees from the Department of Vehicle of National Pingtung University of Science and Technology, Taiwan, in 2023 and 2025, respectively. He is currently an engineer at Wistron Corporation, New Taipei City, Taiwan.



Kuan-Chi Lin received his B.S. and M.S. degrees from the Department of Vehicle of National Pingtung University of Science and Technology, Taiwan, in 2023 and 2025, respectively. He is currently an engineer at United Microelectronics Corporation, Hsinchu, Taiwan.